Sideslip Angle Estimation Based on GPS and Magnetometer Measurements

Jong-Hwa Yoon, Huei Peng
University of Michigan

G036 Lay Automotive Laboratory
Ann Arbor, MI 48109-2133, USA
Phone: 1-734-255-3461
Fax: 1-734-764-4256
E-mail: jongy@umich.edu

This paper proposes a cost-effective method to estimate the vehicle sideslip angle on various frictional surfaces on banked roads. This paper demonstrates that the vehicle sideslip can be estimated by combining measurements of Global Positioning System (GPS), Inertial Measurement Unit (IMU), and a magnetometer in the Kalman filter framework. Among all the measurements, the magnetometer is the most vulnerable to exogenous disturbances. To reject them, a stochastic filter is designed and integrated into the Kalman filter framework. Significant delays in GPS measurements are addressed by "measurement shifting". The performance and accuracy of the proposed method are verified by comprehensive simulations and experiments.

Topics / Sideslip estimation, Kalman Filter, Magnetometer, GPS, Stochastic Filter

1. INTRODUCTION

The vehicle sideslip angle is a critical piece of information for electronic stability control (ESC) systems. The National Highway Traffic Safety Administration (NHTSA) sets its estimation as a requirement for ESC. Since it is not directly measurable using today's on-board sensors, researchers have proposed various methodologies for its estimation [1-7]. These methodologies can be categorized into two groups: dynamic model-based estimation and kinematics-based estimation. Dynamic model-based methods employ a vehicle dynamic model that describes how the estimated sideslip angle is affected by and related to vehicle input signals and parameters, such as steering angle and tire cornering stiffness. These model-based methods require accurate vehicle parameters and are reliable only for the linear range of the sideslip-lateral force relationship such as on high frictional surfaces. Kinematics-based methodologies process on-board sensor signals such as the inertial measurement unit (IMU) to estimate the sideslip angle. As they usually have a much wider range of validity, sideslip angles can be estimated regardless of surface friction levels. However, the accuracy of these methods can be drastically deteriorated by unknown sensor bias or road disturbances such as gravity on a banked road.

Bevly et al. proposed a method utilizing a single antenna GPS along with an IMU for sideslip angle estimation [8-9]. Since the vehicle heading angle is not observable with a single antenna GPS, this method relies on IMU measurement integration to calculate the heading angle. Accordingly, it is vulnerable to unknown sensor bias. In addition, this method does not effectively address out-of-plane vehicle motion such as roll and pitch. Yoon and Peng proposed a new method using two single antenna GPS receivers [10]. This method uses the kinematic relationship between the velocities of two GPS receivers; hence vehicle heading and sideslip angles are calculated directly. However, this method works only for in-plane vehicle motion. Ryu et al. proposed a method using a dual-antenna GPS receiver [11-12]. In this method, the vehicle heading angle is directly measured by detecting the phase shift of carrier waves arriving at two different antennae at known locations on the vehicle. Unlike the aforementioned methodologies, this method can provide accurate sideslip estimations on various frictional surfaces, even on banked roads. However, it is too expensive to be used in production vehicles today[13].

This paper proposes a cost-effective method to estimate the vehicle sideslip angle for a wide range of road surface frictions and bank angles. This method combines measurements of the velocity from a single antenna GPS, the heading from a magnetometer and angle-rate/acceleration from an IMU. Even though a magnetometer can provide direct measurement of vehicle yaw and roll angles, using it for a ground vehicle application is not common due to its high susceptibility to disturbances [14]. This paper introduces a stochastic filter to reject large errors in a magnetometer (hereinafter MAG) measurement. This new filter is integrated into a Kalman filter framework.

We also present a method addressing the significant delays in GPS measurements. This is important because low-cost GPS receivers are known to have significant delays partly due to their low update rates (< 5 Hz)[11-12]. A comprehensive simulation study is conducted using the commercial software CarSim™ to prove the feasibility of the new method. The method is verified by experiments on snow/ice surfaces under several different maneuvers.

2. METHODS

Figure 1 shows the schematic overview of two Kalman filters to estimate the vehicle sideslip angle. The Heading Kalman Filter calculates yaw/roll angles from MAG and IMU measurements. The sideslip angle is then calculated through the Sideslip Kalman Filter by combining GPS and IMU measurements. Given the system,

$$\begin{aligned} x_k &= F_{k-1}x_{k-1} + G_{k-1}u_{k-1} + \Lambda_{k-1}w_{k-1} \\ z_k &= H_k x_k + v_k \end{aligned} \tag{1}$$

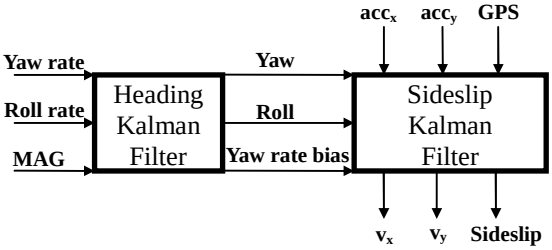

Fig. 1 Schematic diagram of the two Kalman filters

the Kalman filter provides state estimation through Equations (2)-(6) [15].

$$\hat{x}_k^- = F_{k-1}\hat{x}_{k-1}^+ + G_{k-1}u_{k-1} \tag{2}$$

$$P_k^- = F_{k-1}P_{k-1}^+F_{k-1}^{\ T} + \Lambda_{k-1}\varepsilon\left(w_{k-1}w_{k-1}^T\right)\Lambda_{k-1}^{\ T} \tag{3}$$

$$K_k = P_k^- H_k^{\ T}\left[H_k P_k^- H_k^{\ T} + \varepsilon\left(v_k v_k^T\right)\right]^{-1} \tag{4}$$

$$\hat{x}_k^+ = \hat{x}_k^- + K_k\left(z_k - H_k\hat{x}_k^-\right) \tag{5}$$

$$P_k^+ = \left(I - K_k H_k\right)P_k^- \tag{6}$$

where $x_k \in R^{n\times 1}$ is the state, $\hat{x}_k^-$ / $\hat{x}_k^+$ are predicted/corrected state estimates, $u_{k-1} \in R^{l_1\times 1}$ is the input, $w_{k-1} \in R^{l_2\times 1}$ is the plant noise, $v_k \in R^{m\times 1}$ is the measurement noise, $\varepsilon(\cdot)$ denotes the expected value and P_k^- / P_k^+ are predicted/corrected state error covariance. This state estimate is optimal when the plant and measurement noise are Gaussian white. Equations (2) and (3) produce "time updates" whereas (5) and (6) produce the "measurement updates".

2.1 Heading Kalman Filter

The magnetic field measurements in the vehicle-fixed frame are rotations of the Earth magnetic field which is the constant vector pointing to the magnetic North in the Earth-fixed frame. Equation (7) shows their relationship in the ZYX Euler angle definitions. To determine the attitude of a three-dimensional object, at least two independent directional vectors are required. However, since MAG can provide only one vector, the solution of Equation (7) would have redundant answers. This problem is resolved by assuming zero pitch (θ) angle. The negligible pitch angle assumption converts Equation (7) into Equation (8), which is used in our study.

$$\begin{bmatrix} m_x \\ m_y \\ m_z \end{bmatrix} = \begin{bmatrix} \cos\psi\cos\theta & \sin\psi\cos\theta & -\sin\theta \\ -\sin\psi\cos\phi + \cos\psi\sin\theta\sin\phi & \cos\psi\cos\phi + \sin\psi\sin\theta\sin\phi & \cos\theta\sin\phi \\ \sin\psi\sin\phi + \cos\psi\sin\theta\cos\phi & -\cos\psi\sin\phi + \sin\psi\sin\theta\cos\phi & \cos\theta\cos\phi \end{bmatrix} \begin{bmatrix} M_X \\ M_Y \\ M_Z \end{bmatrix} \tag{7}$$

where

$[m_x \quad m_y \quad m_z]^T$ = *magnetic field in a body – fixed frame*

$[M_Z \quad M_Y \quad M_Z]^T$ = *magnetic field in the Earth– fixed frame*

$[\psi \quad \theta \quad \phi]$ = [*yaw pitch roll*]

$$\begin{aligned} m_x &= M_X\cos\psi \\ m_y &= -M_X\sin\psi\cos\phi + M_Z\sin\phi \\ m_z &= M_X\sin\psi\sin\phi + M_Z\cos\phi \end{aligned} \tag{8}$$

For the time update equations of the Heading Kalman Filter, the kinematics for the yaw/roll rates and angles are presented as

$$\begin{bmatrix} \dot{\psi} \\ \dot{b}_r \\ \dot{\phi} \\ \dot{b}_p \end{bmatrix} = \begin{bmatrix} 0 & -1 & 0 & 0 \\ 0 & 0 & 0 & 0 \\ 0 & 0 & 0 & -1 \\ 0 & 0 & 0 & 0 \end{bmatrix} \begin{bmatrix} \psi \\ b_r \\ \phi \\ b_p \end{bmatrix} + \begin{bmatrix} 1 & 0 \\ 0 & 0 \\ 0 & 1 \\ 0 & 0 \end{bmatrix} \begin{bmatrix} r_m \\ p_m \end{bmatrix} + noise \tag{9}$$

where

$[b_r \quad b_p]$ = *bias in yaw/roll rate measurement*

$[r_m \quad p_m]$ = *yaw/roll rate measurement*

noise = *the Gaussian white noise*

The state vector does not contain the pitch angle due to the zero-pitch assumption. Since Equation (8) is nonlinear, the extended Kalman filter technique is used and the Jacobian of Equation (8) with respect to the state is used as H_k in Equation (4).

2.2 Stochastic properties of the MAG disturbance

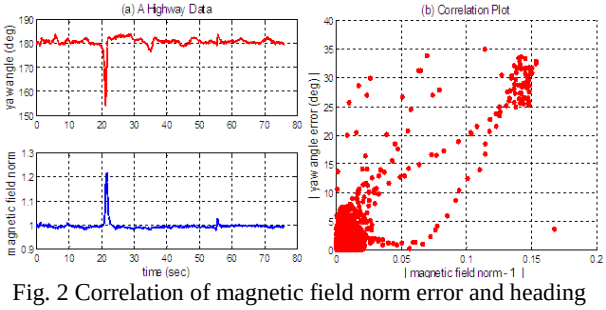

Fig. 2 Correlation of magnetic field norm error and heading angle error

Since the Earth's magnetic field is weak (≈ 60 μT), an adjacent vehicle can induce a significant disturbance in the MAG measurements [14, 16-17]. Figure 2(a) is typical highway test data. The yaw angle is calculated purely from MAG measurements. The yaw angle error observed near the 20 second mark was induced by a passing vehicle. It is worth noting that the norm of the MAG measurement deviates from unity when a disturbance occurs. Absolute values of the heading error and the deviation of the MAG measurement norm from unity for 8 highway data sets are plotted in Figure 2(b). Since the correlation coefficient is 0.9, deviation of the

magnetic field norm from unity can be an effective indicator of a disturbance in MAG measurements.

When disturbances occur, measurement errors (v_k) in Equation (1) are not Gaussian white. As this violates one critical assumption of the Kalman filter, derivation of the Kalman filter is revisited with a new stochastic property of disturbed measurements.

Let w be the disturbance present in the magnetic field measurement. The absolute value of w is assumed to be upper-bounded by b_o. Since no prior knowledge of w is available, its probability density function (PDF) has the Uniform distribution bounded by b_o.

Let two random variables x and z be related via a joint probability density function $f_{X,Z}(x,z)$. For any given z (measurement), the optimal estimation of x minimizing $\varepsilon[(x-\hat{x})^2]$ is

$$\hat{x} = \varepsilon(x \mid z) = \int x \frac{f_{X,Z}(x,z)}{f_Z(z)} dx \tag{10}$$

This is known as the minimum mean square error (MMSE) estimation. For the Bivariate Normal distribution, $\hat{x}$ is expressed as a linear function of z. However, a disturbed measurement (z) has the Uniform distribution, whereas the random variable x (state to be estimated) has the Normal distribution as

$$\begin{aligned} x &= \mu_x + N(0,\sigma) \\ z &= cx + U(-b_1, b_2) \end{aligned} \tag{11}$$

where $\mu_x, c, \sigma, b_1, b_2$ are constants characterizing the probability distributions. Then the MMSE estimation is

$$\hat{x} = \int_{(z-b_2)/c}^{(z+b_1)/c} \left[\frac{x e^{\left(-\frac{1}{2}\left(\frac{x-\mu_x}{\sigma}\right)^2\right)}}{\int_{(z-b_2)/c}^{(z+b_1)/c} e^{\left(-\frac{1}{2}\left(\frac{s-\mu_x}{\sigma}\right)^2\right)} ds} \right] dx \tag{12}$$

which is non-linear. A linear relationship is preferred to be compatible with the Kalman filter framework. For this purpose, the Truncated Normal distribution substitutes for the Uniform distribution because it is a close approximation of the Uniform distribution when the standard deviation is large enough compared to the truncated bound as seen in Figure 3.

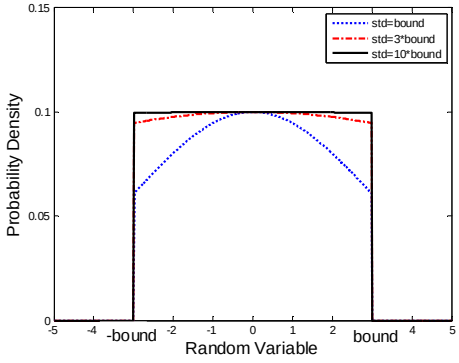

Fig. 3 Truncated Normal distribution under three different standard deviations

If random variable z is truncated by z_b around $\frac{\sigma_z}{\rho\sigma_x}x$, the PDF, MMSE, and variance are presented in Table 1. In Equation (15), the term inside the dash-lined box is a modification factor (denoted as m).

Table 1 Joint Normal and Truncated Normal distribution

PDF $f_{X,Z}(x,z)$

$$\begin{cases} A\exp\left(-\frac{1}{2(1-\rho^2)}\left[\left(\frac{x}{\sigma_x}\right)^2 - 2\rho\left(\frac{x}{\sigma_x}\right)\left(\frac{z}{\sigma_z}\right) + \left(\frac{z}{\sigma_z}\right)^2\right]\right), & f \left| z - \frac{\sigma_z}{\rho\sigma_x}x \right| \le z_b \\ 0, & Otherwise \end{cases} \tag{13}$$

$$where\ A = \frac{1}{2\pi\sigma_x\sigma_z\sqrt{1-\rho^2}\left[\Phi\left(\frac{x_b}{\sigma_x\sqrt{1-\rho^2}}\right) - \Phi\left(\frac{-x_b}{\sigma_x\sqrt{1-\rho^2}}\right)\right]}$$

$$\rho = \frac{\sigma_{XZ}}{\sigma_X\sigma_Z},\quad \phi(x) = \frac{1}{\sqrt{2\pi}}e^{-\frac{1}{2}x^2},\quad and\ \Phi(x) = \int_{-\infty}^{x}\phi(t)dt$$

MMSE $\hat{x} = \varepsilon(x \mid z)$

$$\rho\frac{\sigma_x}{\sigma_z}z \tag{14}$$

Variance $\int_{-\infty}^{\infty}\int_{-\infty}^{\infty}(z-\hat{z})^2 f_{X,Z}(x,z)dxdz$

$$\sigma_z^2(1-\rho^2)\left[\frac{1}{\Phi(\zeta)-\Phi(-\zeta)} + \frac{2\zeta\phi(\zeta)}{\{\Phi(\zeta)-\Phi(-\zeta)\}^2}\right] \mathbf{m} \tag{15}$$

$$where$$

$$\zeta = \frac{z_b}{\sigma_z\sqrt{1-\rho^2}},\quad and\quad \hat{z} = \frac{\sigma_z}{\rho\sigma_x}\hat{x}$$

2.3 Integration on the Kalman filter framework

Equations (14)-(15) are identical to MMSE and variance of Bivariate Normal distribution whose standard deviations are $\sigma_x\sqrt{m}$ and $\sigma_z\sqrt{m}$, respectively. This suggests that when the j[th] component of a measurement vector (standard deviation of σ_j) is disturbed, it can be treated as the Gaussian white noise whose standard deviation is $\sigma_j\sqrt{m_j}$. Therefore, $\varepsilon(v_k v_k^T)$ of Equation (4) is expressed as

$$\varepsilon(v_k v_k^T) = \begin{bmatrix} \sigma_1^2 & & & \\ & \ddots & & \\ & & \sigma_j^2 & \\ & & & \ddots \\ & & & & \sigma_m^2 \end{bmatrix} \begin{bmatrix} 1 & & & \\ & \ddots & & \\ & & m_j & \\ & & & \ddots \\ & & & & 1 \end{bmatrix} = RM \tag{16}$$

where each measurement error component is assumed to be uncorrelated with each other. R is the measurement error covariance matrix and M is the modification matrix. When measurements are not disturbed, M would be the identity matrix, which is equivalent to the Kalman filter. Otherwise, the corresponding components of M are calculated by Equation (15).

2.4 Sideslip Kalman filter

This Kalman filter combines the longitudinal/lateral accelerations from an IMU, the velocities from a single GPS receiver, and yaw/roll angles from the Heading Kalman Filter. In the ISO coordinate system, the kinematics relating accelerations and velocities of an IMU are

$$a_{m,x} = \dot{U} - \dot{\psi}V + b_x + w_x$$
$$a_{m,y} = \dot{V} + \dot{\psi}U + b_y + g\sin\phi + w_y \quad (17)$$

where

$[a_{m,x} \quad a_{m,y}]$ = *longitudinal / lateral acceleration measuements*
$[U \quad V]$ = *longitudinal / lateral velocities*
$[b_x \quad b_y]$ = *biases in* $[a_{m,x} \quad a_{m,y}]$
$g\sin\phi$ = *gravitational compoment by roll*
$[w_x \quad w_y]$ = *the Gaussian white noise*

Since yaw rate ($\dot{\psi}$) is known by subtracting the yaw rate bias (calculated from the heading Kalman filter) from yaw rate measurements, Equation (17) is rearranged to form the time update equation as

$$\begin{bmatrix}\dot{U}\\ \dot{b}_x\\ \dot{V}\\ \dot{b}_y\end{bmatrix} = \begin{bmatrix}0 & -1 & \dot{\psi} & 0\\ 0 & 0 & 0 & 0\\ -\dot{\psi} & 0 & 0 & -1\\ 0 & 0 & 0 & 0\end{bmatrix}\begin{bmatrix}U\\ b_x\\ V\\ b_y\end{bmatrix} + \begin{bmatrix}1 & 0\\ 0 & 0\\ 0 & 1\\ 0 & 0\end{bmatrix}\begin{bmatrix}a_{m,x}\\ a_{m,y} - g\sin\phi\end{bmatrix} + noise \quad (18)$$

Velocities from a GPS receiver are converted into longitudinal, lateral, and vertical velocities via

$$\begin{bmatrix}U^{GPS}\\ V^{GPS}\\ V^{GPS}{}_v\end{bmatrix} = \begin{bmatrix}\cos\psi & \sin\psi & 0\\ -\cos\phi\sin\psi & \cos\phi\cos\psi & \sin\phi\\ \sin\phi\sin\psi & -\sin\phi\cos\psi & \cos\phi\end{bmatrix}\begin{bmatrix}V^{GPS}{}_X\\ V^{GPS}{}_Y\\ V^{GPS}{}_Z\end{bmatrix} \quad (19)$$

where

$[V_X^{GPS} \; V_Y^{GPS} \; V_Z^{GPS}]$ = *velocities of a GPS receiver in the Earth – fixed frame*
$[U^{GPS} \; V^{GPS} \; V_v^{GPS}]$ = *longitudinal / lateral / vertical velocities of a GPS receiver in the vehicle – fixed frame*

ψ and ϕ are provided by the heading Kalman filter. When GPS updates are available, measurement update equations are

$$\begin{bmatrix}U^{GPS}\\ V^{GPS}\end{bmatrix} = \begin{bmatrix}1 & 0 & 0 & 0\\ 0 & 0 & 1 & 0\end{bmatrix}\begin{bmatrix}U\\ b_x\\ V\\ b_y\end{bmatrix} + noise \quad (20)$$

2.5 GPS delay handling

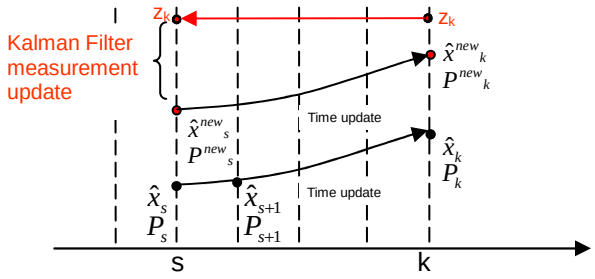

Fig. 4 Discrete Kalman filter framework to handle delays

$[U^{GPS} \; V^{GPS}]$ in Equation (20) have significant delays inherited from the property of a low-cost GPS[10-12]. A method similar to what Larsen proposed [18] is implemented. Figure 4 shows a discrete time Kalman filter framework to address delays. From time step s to k, state estimation and its covariance are evolved only through the time update because GPS measurements are unavailable. At time step k, GPS measurement is available (z_k) but it represents a value of time s due to the delay. Accordingly z_k is shifted back to time s and merged with state estimation of $\hat{x}_s$ to yield the measurement updated state of $\hat{x}_s^{new}$. Then the new state at k ($\hat{x}_k^{new}$) is obtained through time update from $\hat{x}_s^{new}$.

3. RESULTS

3.1 Simulations

A comprehensive simulation was run with Carsim™. Four types of maneuvers (single lane change, double lane change, slalom, and J-turn) are combined with two different surface friction levels (asphalt and ice) and two road types (flat and banked). Figure 5 shows the simulation layout. Black lines represent asphalt and cyan blue lines are for ice. Dotted lines mean banked roads where solid lines are flat surfaces. Table 2 summarizes the simulated errors of all sensors. In addition to injecting white noise, the IMU had biases, the GPS had a delay, and the magnetometer had random disturbances.

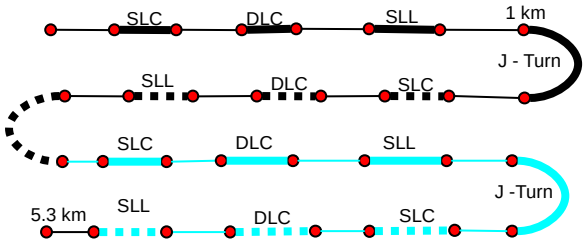

Fig. 5 The simulation layout

Table 2 Summary of simulated error

Sensor	Simulated Error
IMU	- **Standard deviation of white noise** 0.01 m/s^2 for accelerations 0.1 deg/sec for gyros - **Injected bias** 0.5 m/s^2 for accelerations 2 deg/sec for gyros
GPS	- **Standard deviation of white noise** 0.01 m/s - **Delay** 400 ms
Magnetometer	- **Standard deviation of white noise** 0.02 - **Disturbances** 12 occurrences at random timing with random magnitude in [0.5,2.0]

Figure 6 shows the vehicle sideslip, yaw, and roll angle estimation of the simulation. Blue dotted lines are estimations and red solid lines are references as true values. Several peaks of MAG norm in Figure 6(a) indicate the occurrences of magnetic disturbances. Even with magnetic disturbances, the vehicle sideslip estimation stays close to the true values throughout the whole time (Figure 6(b)). This suggests the magnetic the disturbance rejection logic effectively functions. In Figure 6(b), four areas are identified as A: flat asphalt, B: banked asphalt, C: flat ice, and D: banked ice surfaces. Accurate sideslip estimations in area A and C prove the robustness of the proposed method to different surface friction levels. Additionally, desirable performances of area B and D demonstrate that the method works even on baked roads. This is possible because vehicle roll angles are accurately estimated by

the method (Figure 6(d)). The dotted green line in Figure 6(c) is the yaw angle estimation without the magnetic disturbance rejecting modification. Significant errors of dotted green lines suggest that MAG disturbance is effectively rejected by the method.

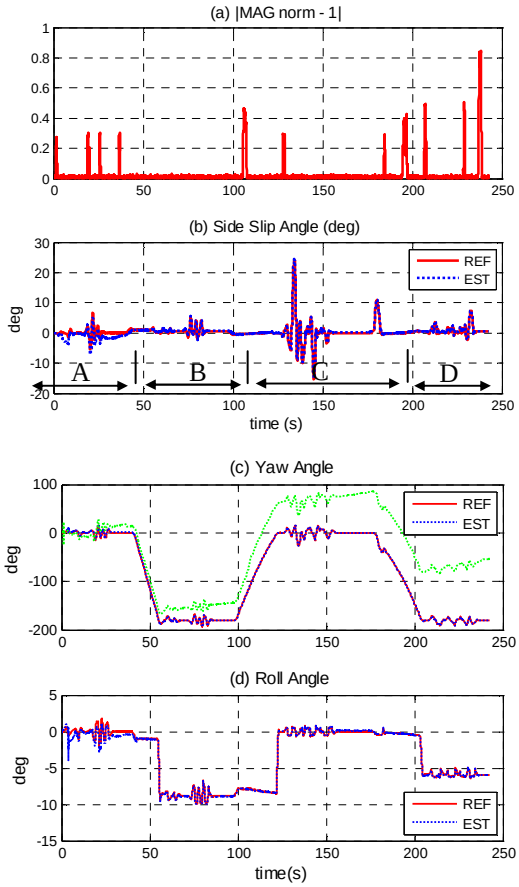

Fig. 6 Vehicle sideslip, yaw and roll angle estimations with the presence of random magnetic disturbances

3.2 Experimental Verifications

A GM Silverado truck is used for experimental verification. Four types of maneuvers (single lane change, double lane change, slalom, and J-turn) were run on packed snow and ice surfaces at the TRW Winter Test Track in Raco, Michigan. Two different vehicle speeds representing fast (90 KPH on snow, 50 KPH on ice) and slow (60 KPH on snow, 30 KPH on ice) were executed. Each driving scenario had 5 runs; a total of 70 data sets were collected. An Xsens MTi magnetometer and an IMU from a production ESC unit (TRW) were used. An Oxford RT2500, with a single GPS receiver, was installed for the reference signal. The vehicle with installed equipment is shown in Figure 7.

Fig. 7 Setup on the experimental vehicle

The experimental data processing uses GPS signals from the RT2500. To mimic a low-cost GPS receiver signal, a 400 ms delay is injected and the data are re-sampled at 5 Hz. Figure 8 shows typical traces of experimental data. As seen in the figure, sideslip estimation stays close to the reference signal. J-Turn sideslip angle estimation shows deviation at the end of the run because that is when the vehicle slows down significantly. Errors in sideslip estimation due to GPS noise grows as a vehicle's speed reduces[8]. The sideslip RMS error from 70 collected data is 1.3°.

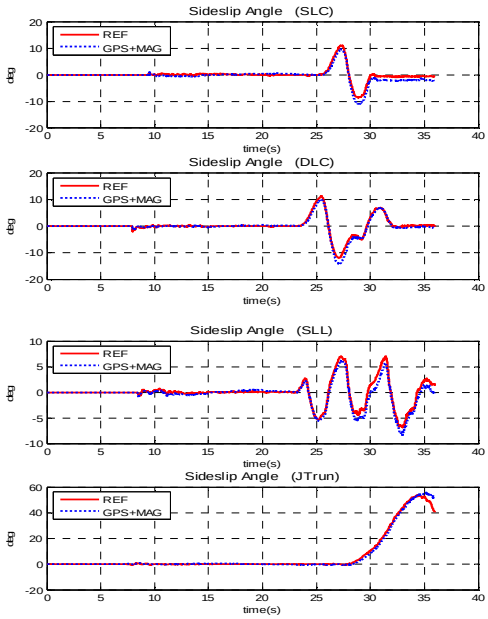

Fig. 8 Experimental sideslip estimation performance (single lane change, double lane change, slalom and J-turn)

As the test track environments were MAG-noise free, on-tract data process does not verify MAG disturbance rejection logic. To verify MAG disturbance rejecting capability, randomly generated MAG disturbances (norm magnitude of [0.05, 1] at 20% occurrence rate) are injected into the on-tract data. The statistical property of the disturbance is chosen based upon actual highway data. With the disturbances, the sideslip RMS error from 70 data sets becomes 1.98°, which is 0.68° worse than the MAG disturbance-free data. For further statistical analysis on MAG disturbance rejection logic, a representative data of each maneuver is selected and the data is processed twenty times with randomly generated MAG disturbances of various magnitudes and frequencies. The results are shown in Figure 9. Red lines are the reference signals, blue lines are estimations, and green lines are estimation without MAG disturbance rejection modification (M in Equation (16)). As seen in the figure, the proposed method successfully rejects MAG disturbances. The RMS error from 80 data sets (4 selected data × 20 runs each) is 1.28° with a MAG disturbance of [0.05, 1] at 20% occurrence rate. Performance is similar with MAG disturbance of [1,2] at 20 % occurrence rate. However, a 40% occurrence rate has the performance value of 2.23°.

Figure 10 shows traces of roll angle estimation of the method; the estimation follows the reference signal accurately. The RMS errors from 70 data sets are calculated, and without the MAG disturbances, it is 0.81°. With the simulated MAG disturbances, it slightly

increases to 0.84°.

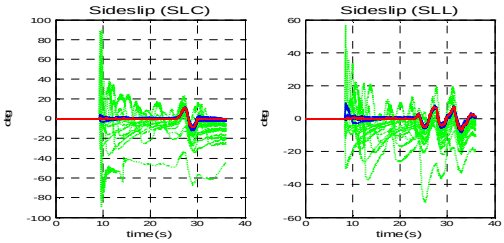

Fig. 9 Experimental sideslip estimation performance with randomly generated MAG disturbances (20 runs each)

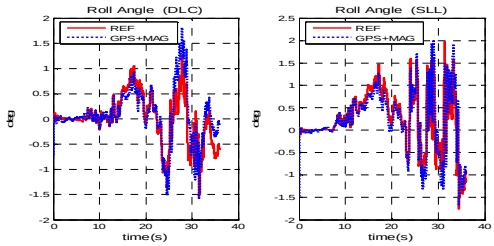

Fig. 10 Experimental roll angle estimation performance

5. CONCLUSION

This paper shows that the vehicle sideslip angle can be estimated by combining measurements from a GPS, a magnetometer, and an IMU. The Kalman filter is employed for sensor fusion. To reject magnetic field disturbances, a new stochastic filter is designed based on the joint Normal and Truncated Normal distribution and fitted into the Kalman filter framework.

Comprehensive simulations show that the sideslip estimation stays accurate regardless of surface friction type, road bank, and magnetic field disturbances. Experimental results verify that the estimation performance is acceptable for various maneuvers. The RMS error is 1.3°, but it increases to 2.23° with significant amount of MAG disturbances. Disturbance occurrence rates have more impact on the performance than disturbance magnitudes. Experimental data also show that the proposed method can estimate vehicle roll angles accurately.

ACKNOWLEDGEMENTS

The authors would like to thank TRW Automotive for sponsoring this research. Special thanks to Danny Milot of TRW Automotive for his encouragement and support, and Dr. Mark Elwell for his technical advice.

REFERENCES

[1] J. Farrelly and P. Wellstead, "Esitmation of Vehicle Lateral Velocity," in *IEEE International Conference on Control Applications*, Dearborn, MI, USA, 1996, pp. 552-557.

[2] U. Kiencke and A. Daiss, "Observation of Lateral Vehicle Dynamics," *Control Engineering Practice*, vol. 5, pp. 1145-1150, 1997.

[3] M. C. Best, *et al.*, "An Extended Adaptive Kalman Filter for Real-time State Estimation of Vehicle Handling Dynamics," *Vehicle System Dynamics*, vol. 34, pp. 57-75, 2000.

[4] A. Nishio and K. Tozu, "Development of Vehicle Stability Control System Based on Vehicle Sideslip Angle Estimation," presented at the SAE, New York, 2001.

[5] H. Cherouat, *et al.*, "Vehicle velocity, side slip angles and yaw rate estimation," presented at the IEEE ISIE, Dubrovnik, Croatia, 2005.

[6] L. Imsland, *et al.*, "Vehicle Velocity Estimation using Modular Nonlinear Observers," *Automatica*, vol. 42, pp. 2091-2103, 2006.

[7] X. Gao and Z. Yu, "Vehicle Sideslip Angel Estimation by using High Gain Observer," in *AVEC 9th International Symposium on Advanced Vehicle Control*, Kobe, Japan, 2008.

[8] D. M. Bevly, "Global Positioning System (GPS): A Low-Cost Velocity Sensor for Correcdting Inertial Sensor Errors on Ground Vehicles," *Journal of Dynamic System, Measurement, and Control*, vol. 126, pp. 255-264, 2004.

[9] D. M. Bevly, *et al.*, "The Use of GPS Based Velocity Measurements for Measurement of Sideslip and Wheel slip," *Vehicle System Dynamics*, vol. 38, pp. 127-147, 2003.

[10] J.-H. Yoon and H. Peng, "Vehicle Sideslip Angle Estimation Using Two Single-Antenna GPS Receivers," in *Dynamic System Control Conference*, Boston, MA, 2010.

[11] J. Ryu and J. C. Gerdes, "Integrating Inertial Sensors with GPS for Vehicle Dynamics Control," *Journal of Dynamic System, Measurement, and Control*, vol. 126, pp. 243-254, 2004.

[12] J. Ryu, *et al.*, "Vehicle Sideslip and Roll Parameter Estimation Using GPS," in *AVEC 6th International Symposium on Advanced Vehicle Control*, Hiroshima,Japan, 2002.

[13] D. Piyabongkarn, *et al.*, "Development and Experimental Evaluation of A Slip Angle Estimator for Vehicle Stability Control," in *Proceeding of the 2006 American Control Conference*, Minneapolis, Minnesota, 2006.

[14] E. Abbott and J. D. Powell, "Land-Vehicle Navigation Using GPS," in *Proceedings of the IEEE*, 1999, pp. 145-162.

[15] M. *: Theory and Practice*: Prentice-Hall, Inc., 1993.

[16] P. Ripka, *Magnetic sensors and magnetometers*: Artech House, 2001.

[17] S. Taghvaeeyan and R. Rajamani. (2001, Use of vehicle magnetic signatures for position estimation. *Applied Physics Letters 99(134101)*.

[18] T. D. Larsen, *et al.*, "Incorporation of time delayed measurements in a Discrete-time Kalman Filter," in *Proceedings of the 37th IEEE conference on Decision & Control*, Tampa, Florida, 1998, pp. 3972-3977.